ACS APPLIED MATERIALS & INTERFACES

Research Article

www.acsami.org

Dissolution Chemistry and Biocompatibility of Silicon- and Germanium-Based Semiconductors for Transient Electronics

Seung-Kyun Kang,[†,‡] Gayoung Park,[§,‡,△] Kyungmin Kim,[†,‡] Suk-Won Hwang,[∥] Huanyu Cheng,[†,◇] Jiho Shin,[¶] Sangjin Chung,[†] Minjin Kim,[⊥] Lan Yin,[†] Jeong Chul Lee,*[,†] Kyung-Mi Lee,*[,§,#] and John A. Rogers*[,†]

[†]Frederick Seitz Materials Research Laboratory, Department of Materials Science and Engineering, Beckman Institute for Advanced Science and Technology, and [¶]Department of Chemical and Biomolecular Engineering, University of Illinois at Urbana−Champaign, Urbana, Illinois 61801, United States

[§]Global Research Laboratory, Department of Biochemistry and Molecular Biology, Korea University College of Medicine, Seoul 136-713, Republic of Korea

[∥]KU-KIST Graduate School of Converging Science and Technology, Korea University, Seoul 136-701, Republic of Korea

[⊥]KIER-UNIST Advanced Center for Energy, Korea Institute of Energy Research, Daejeon 305-343, Republic of Korea

[#]Department of Melanoma Medical Oncology and Immunology, MD Anderson Cancer Center, Houston, Texas 77054, United States

[△]Department of Biomicrosystem Technology, Korea University, Seoul 136-713, Republic of Korea

Supporting Information

ABSTRACT: Semiconducting materials are central to the development of high-performance electronics that are capable of dissolving completely when immersed in aqueous solutions, groundwater, or biofluids, for applications in temporary biomedical implants, environmentally degradable sensors, and other systems. The results reported here include comprehensive studies of the dissolution by hydrolysis of polycrystalline silicon, amorphous silicon, silicon−germanium, and germanium in aqueous solutions of various pH values and temperatures. In vitro cellular toxicity evaluations demonstrate the biocompatibility of the materials and end products of dissolution, thereby supporting their potential for use in biodegradable electronics. A fully dissolvable thin-film solar cell illustrates the ability to integrate these semiconductors into functional systems.

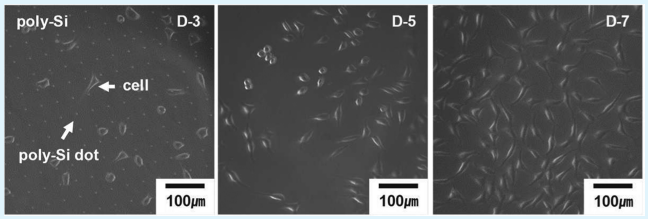

KEYWORDS: *transient electronics, dissoluble semiconductors, bioresorbable electronics, biocompatible materials, thin-film solar cells*

1. INTRODUCTION

Electronic systems designed to partially or fully dissolve in aqueous solutions with predictable and controlled kinetics are of growing interest for bioresorbable implants, ecofriendly sensors, consumer devices with minimized hazardous waste streams, hardware-secure electronics, and other devices.[1−19] Such classes of physically *transient electronics* are of particular relevance in biomedicine, where they have the potential for use in programmable drug delivery, temporary cardiac pacemaking and nerve stimulation, and in sensors for medical therapy, diagnosis, and monitoring.[1,2,19−22] Dissolvable materials that are biocompatible and have biocompatible end products are critically important for such systems. Previous studies establish options that include nanomembranes of monocrystalline silicon (Si NMs) and thin films of ZnO for the semiconductors,[1−3,7] metals and metal alloys (Mg, Mg alloy, Fe, Fe alloy, Zn, W, and Mo) for the conductors,[4,5] various oxides (SiO_2, SiN_x, and MgO) for the interlayer and gate dielectrics and encapsulants,[6] and polymers and metal foils for the substrates and superstrates.[5,8] The hydrolysis mechanisms for these inorganic materials appear in the Supporting Information (SI).

Here we investigate the dissolution behavior and biocompatibility of several additional semiconductors with utility in this context, including polycrystalline silicon (poly-Si), amorphous silicon (a-Si), alloys of silicon and germanium (SiGe), and Ge itself. These materials are attractive in part because of their extensive use in conventional electronics technologies. Poly-Si, for example, until the recent introduction of metal gate technology, served as the gate material in metal oxide−semiconductor field-effect transistors and complementary metal oxide−semiconductor circuits.[23] Both poly-Si and a-Si are found in solar cells and in active matrix display backplanes.[23,24] SiGe is used extensively in heterojunction bipolar transistors with high-frequency performance and extensive applications in personal communication devices such as digital wireless handsets, as well as other entertainment and information technologies like digital set-top boxes, direct broadcast satellite, automobile collision avoidance systems, and personal digital

Received: March 22, 2015
Accepted: April 13, 2015
Published: April 13, 2015

DOI: 10.1021/acsami.5b02526
ACS Appl. Mater. Interfaces 2015, 7, 9297−9305

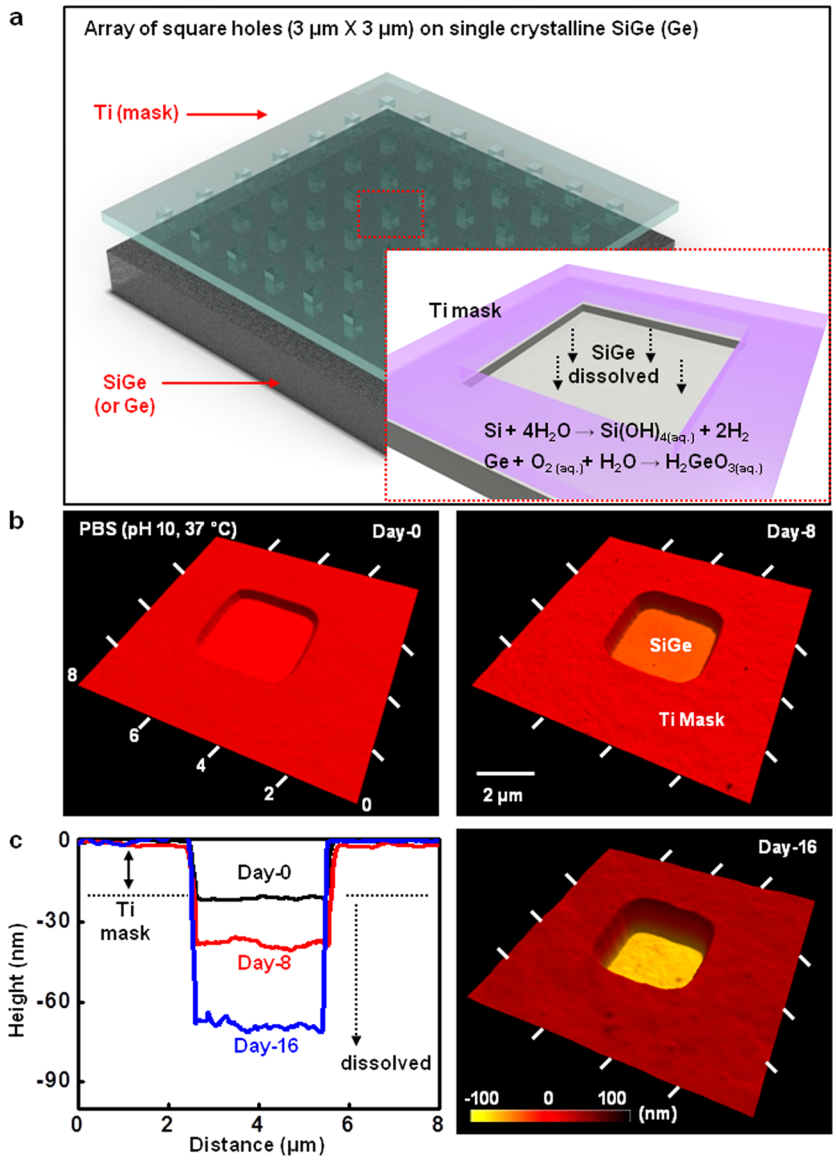

Figure 1. Schematic illustration and experimental results for dissolution tests on SiGe and Ge. (a) Array of patterned square openings (3 μm × 3 μm × 30 nm) formed using layers of Ti (~30 nm thick) on single-crystalline SiGe(100) and Ge(100) wafers. Inset: magnified view of the test structure and dissolution mechanisms of SiGe. (b) Series of AFM topographical images at different stages of hydrolysis in a buffer solution (pH 10) at physiological temperature (37 °C) after day 0 (top left), day 8 (top right), and day 16 (bottom right), respectively. (c) Corresponding profiles of a representative patterned hole of SiGe at the same conditions (black, day 0; red, day 8; blue, day 16).

assistants.[25,26] Ge served as the basis for the earliest transistors, with smaller band gap and larger minority-carrier mobility compared to silicon, resulting in smaller transit time and higher speed of operation, of relevance to high-frequency devices.[27] The following describes the comprehensive dissolution testing and in vitro cell-based biocompatibility evaluation of these materials; the results establish their ability to serve as semiconductors for bio- and ecoresorbable forms of transient electronics.

2. RESULTS AND DISCUSSION

2.1. Dissolution Kinetics. Previous work describes the hydrolysis of monocrystalline silicon (mono-Si) and porous silicon (p-Si), wherein the governing chemical reaction is $Si + 4H_2O \rightarrow Si(OH)_4(aq) + 2H_2$.[1,2,7] Ge is known to react in aqueous solutions that contain dissolved oxygen, i.e., $Ge + O_2(aq) + H_2O \rightarrow H_2GeO_3(aq)$.[28] Recent systematic studies of the hydrolysis of mono-Si(100) in solutions with different pH values (between 6 and 10), ion concentrations, and temperatures indicate dissolution rates in the range of 0.5−624 nm/day, for low or modest doping levels in the Si.[2] These values are well within a range that leads to the complete disappearance of ultrathin (~300 nm or less) sheets of mono-Si (i.e., nanomembranes) on time scales that are relevant for many envisioned uses in bioresorbable electronics. Separate investigations of poly-Si and a-Si and of SiGe and Ge are needed to assess their suitability for similar applications.

Systematic dissolution tests for poly-Si, a-Si, monocrystalline SiGe [$Si_8Ge_2(100)$], and monocrystalline Ge [Ge(100)] used aqueous buffer solutions (Sigma-Aldrich, USA) with pH values between 7 and 10, at room and physiological (37 °C) temperatures. The studies of poly-Si and a-Si involved measurements of changes in the thicknesses of a patterned array of squares (3 μm × 3 μm × 100 nm) of material formed

DOI: 10.1021/acsami.5b02526
ACS Appl. Mater. Interfaces 2015, 7, 9297−9305

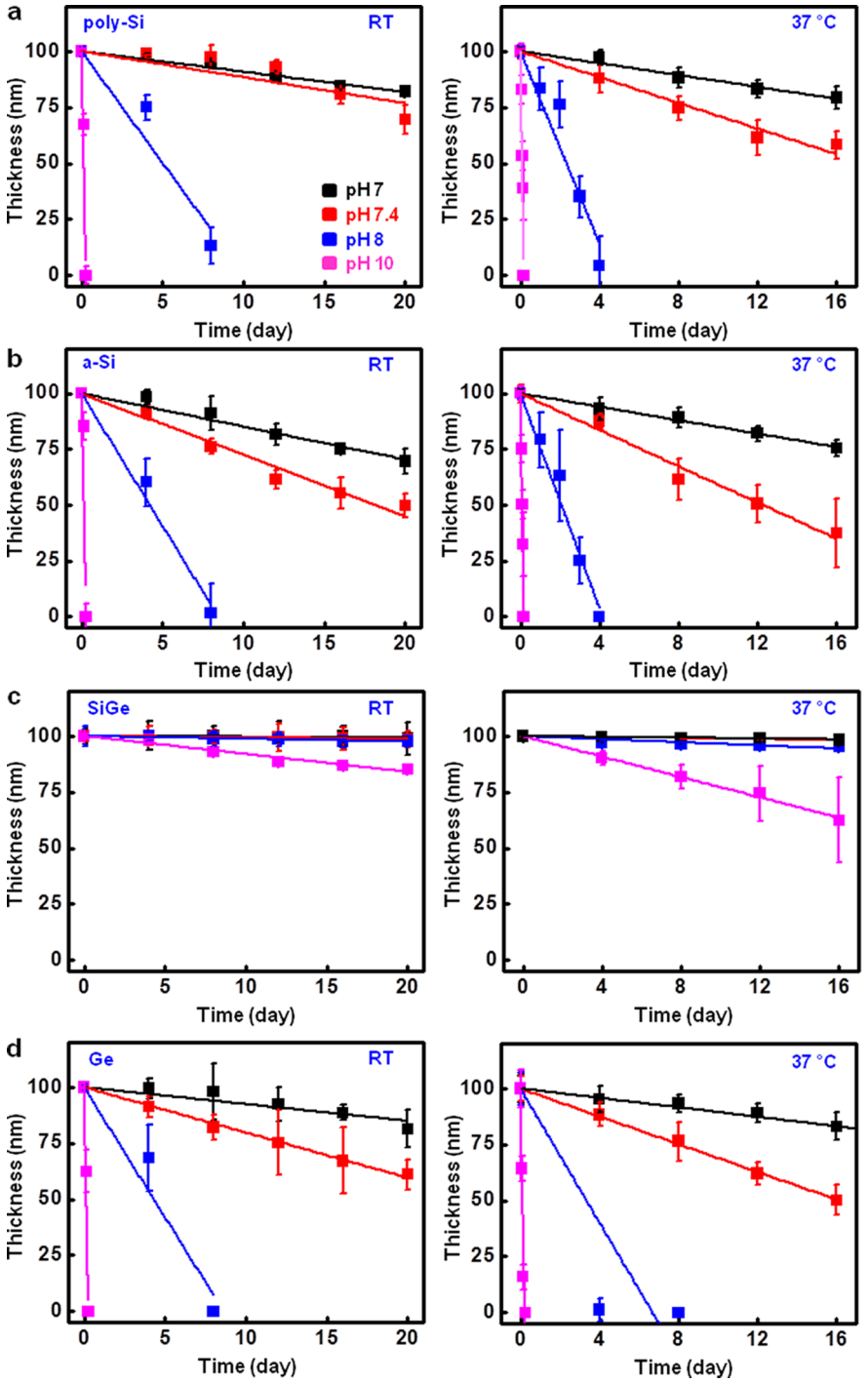

Figure 2. Dissolution studies of various semiconducting materials (p-Si, a-Si, SiGe, and Ge) in diverse aqueous solutions, with different pH values and temperatures. Theoretical (lines) and experimental (symbols) results for the time-dependent dissolution studies of (a) poly-Si, (b) a-Si, (c) SiGe, and (d) Ge in buffer solutions (black, pH 7; red, pH 7.4; blue, pH 8; purple, pH 10) at room (left) and physiological (right, 37 °C) temperature.

on a layer of thermal oxide on a Si wafer. (The rate for dissolution of thermal oxide is negligible compared to that for either poly-Si or a-Si at the levels of doping examined here.[1,2,6,7]) Studies of SiGe and Ge relied on wafers (MTI Corp., USA) configured as shown in Figure 1a. Here, a layer of titanium (Ti; ∼30 nm, insoluble in the solutions examined here) with an array of square openings (3 μm × 3 μm) allows selective exposure of the underlying SiGe and Ge to surrounding solutions. Measurements of the time-dependent change in height between the top surface of the Ti and the exposed SiGe and Ge define the dissolution rates. Figures 1b,c and S1 in the SI show the corresponding surface topography and height profiles at various stages of dissolution in a buffer solution with pH 10 at 37 °C.

Parts a−d of Figure 2 summarize the dissolution kinetics for poly-Si, a-Si, SiGe, and Ge. In all cases, the rates at physiological temperature (37 °C) are higher than those at room temperature, as expected.[1] Previous reports suggest that an

DOI: 10.1021/acsami.5b02526
ACS Appl. Mater. Interfaces 2015, 7, 9297−9305

increase in the concentration of OH^- accelerates the dissolution of mono-Si.[2,7] Figure S2 in the SI shows the dependence of the dissolution rate, R, on the pH for poly-Si, a-Si, SiGe, and Ge. Reports on Si etching at relatively high pH suggest that R can be written as $R = k_0[H_2O]^4[OH^-]^{0.25}e^{-(E_A/k_BT)}$, where k_B, E_A, and k_0 are the Boltzmann constant, activation energy, and reaction constant, respectively [here k_0 is 2480 μm/h × $(mol/L)^{-4.25}$].[2,29,30] This same equation does not fully describe the results reported here, as summarized in Figure S2a in the SI and Table 1 and in previous dissolution studies of mono-Si.[2] A generalization of this model, $R = k_0[H_2O]^4[OH^-]^x e^{-(E_A/k_BT)}$, can, however, capture the pH-dependent dissolution of mono-Si, where fitted values of x fall in the range of 0.46−0.90.[2] Figure S2b in the SI shows that this model also accounts for the pH-dependent dissolution behavior of poly-Si, a-Si, SiGe, and Ge from pH 7 to 10. Table 2 summarizes the two constants of this generalized reaction model determined by fitting data at both room and body temperatures. We note that the concentrations of ions such as Cl^- and PO_4^{3-} likely influence the values of E_A and k_0, as for the case of mono-Si.[29]

Table 1. Constants of the Reaction Model of pH-Dependent Dissolution

	poly-Si	a-Si	SiGe	Ge
E_A, eV	0.778	0.768	0.860	0.776

Table 2. Constants of the Generalized Reaction Model of pH-Dependent Dissolution

	poly-Si	a-Si	SiGe	Ge
E_A, eV	0.524	0.518	0.763	0.515
x	0.874	0.865	0.485	0.891

The values of R for poly-Si, a-Si, SiGe, and Ge are 2.8, 4.1, 0.1, and 3.1 nm/day, respectively, in buffer solutions at pH 7.4 and 37 °C. Poly-Si dissolves at a rate similar to that observed for mono-Si (2.9 nm/day), while a-Si and Ge dissolve somewhat more quickly. The reduced density of a-Si facilitates diffusion, thereby accelerating the rate of dissolution.[6] By contrast, SiGe dissolves ∼30 times more slowly than mono-Si. A relevant observation is that the etching rate of Si_8Ge_2 is ∼100 times slower than that of mono-Si at high pH in KOH solutions.[31,32] (The etching rate depends strongly on the temperature and concentration of KOH: the value decreases by ∼200 times in KOH/H_2O = 515 g/1000 mL at 60 °C and ∼1250 times in KOH/H_2O = 130 g/1000 mL at 85 °C for Si with 1.5×10^{22} cm^{-3} Ge.[31,32])

Figure S3 in the SI shows examples of dissolution in biofluids. Even at similar pH, bovine serum (Sigma-Aldrich, USA) leads to dissolution rates at 37 °C that are 30−40 times higher than those of a phosphate buffer solution (0.1 M; Sigma-Aldrich, USA), for poly-Si, a-Si, and mono-Si. The dissolution rate for SiGe exhibits an even more strongly accelerated rate (∼185 times) in bovine serum. Dissolution of Ge is faster (∼10 times) than SiGe but slower than Si.

2.2. In Vitro Biocompatibility Evaluations. Biocompatibility of the materials themselves and the products of their dissolution are important for applications in bioresorbable electronics. Previous studies using cell cultures on mono-Si metastatic breast cancer cells (MDA-MB-231) and on p-Si and p-Ge (porous Ge) with Chinese hamster ovary cells reveal an absence of cytotoxic effects.[33,34] In this study, we used two different cell lines to assess tissue cytotoxicity not only on neighboring stromal fibroblast cells but also on infiltrating immune cells. L929 mouse fibroblast cell lines and whole splenocytes harvested from mouse spleen served as surrogates for the cells in contact with the implanted devices. The following summarizes similar studies on poly-Si, a-Si, SiGe, Ge and mono-Si using a surrogate fibroblast line, L929 cells, seeded directly onto the surfaces of sterilized samples with designs similar to those used in the dissolution tests of the previous section. Polyurethane containing 0.1% zinc diethyldithiocarbamate (ZDEC), which is known to be toxic to cells, acts as positive control. High-density polyethylene (HDPE) and cultures without any added materials serve as negative controls, with no adverse effects on the cells.[35] Details of the experimental setup appear in the Experimental Section. Figure 3a shows the growth and proliferation behavior of the cells and the dissolution of poly-Si observed by phase-contrast microscopy (above) and live/dead assays by fluorescence imaging (below), where the living and dead cells are green and red, respectively. Similar results for a-Si, mono-Si, SiGe, and Ge appear in Figures S4 and S5 in the SI. For all samples, most L929 cells attach tightly to the surfaces of the materials and spread effectively during the culture period. After day 7 of culture, the live/dead assay exhibits viability for most cells and clusters with extended lamellipodia, suggesting no adverse effects on proliferation. Figure 3b summarizes the viability determined by a live/dead cell count from three different areas on each sample. The viability of L929 fibroblasts is high for all materials, showing little signature of toxicity. The poly-Si, a-Si, and mono-Si squares completely disappear between day 3 and 5, consistent with observations of samples without cells (∼3 days) (Figure S6 in the SI).

Cells stained with annexin V/7-AAD and analyzed by flow cytometry confirm expected apoptosis behavior for 72 h.[36] Figures 3c and S7a in the SI present the apoptotic cell distribution for poly-Si, a-Si, SiGe, Ge, and mono-Si and control samples (no material, HDPE, and PU-ZDEC). Annexin V−/7-ADD−, annexin V+/7-ADD−, annexin V+/7-ADD+, and annexin V−/7-ADD+ correspond to viable, early apoptotic, late apoptotic, and dead cells, respectively. No significant increase of apoptosis appears after 72 h of culture for poly-Si, a-Si, SiGe, and Ge compared to the control samples. Mono-Si does not show significant early apoptosis, although the percentage of late apoptotic cells indicates a slight increase (∼12%) over the case of no material and HDPE controls (Figure S7a in the SI). Compared to PU-ZDEC, which causes over 90% of late apoptosis, the extent of apoptosis by mono-Si is low (Figure S7a in the SI).

For further confirmation of biocompatibility under physiological conditions, immune cells in the spleen were harvested, seeded, and cultured on samples for 72 h. Figure S7b in the SI shows no significant changes in the percentage of early or late apoptosis compared to negative (no material, HDPE) and positive (PU-ZDEC) controls. Figure S7 in the SI, which indicates the high viability of splenocytes, also supports this lack of toxicity. (The relatively high pcercentage of dead cells in the spleen is normal because it is the center for removal of old and exhausted immune cells.[37])

A final set of studies focused on assessment of the cytotoxicity of dissolved and extractable components from the solution. Here, extracts consisted of a culture medium used to

DOI: 10.1021/acsami.5b02526
ACS Appl. Mater. Interfaces 2015, 7, 9297−9305

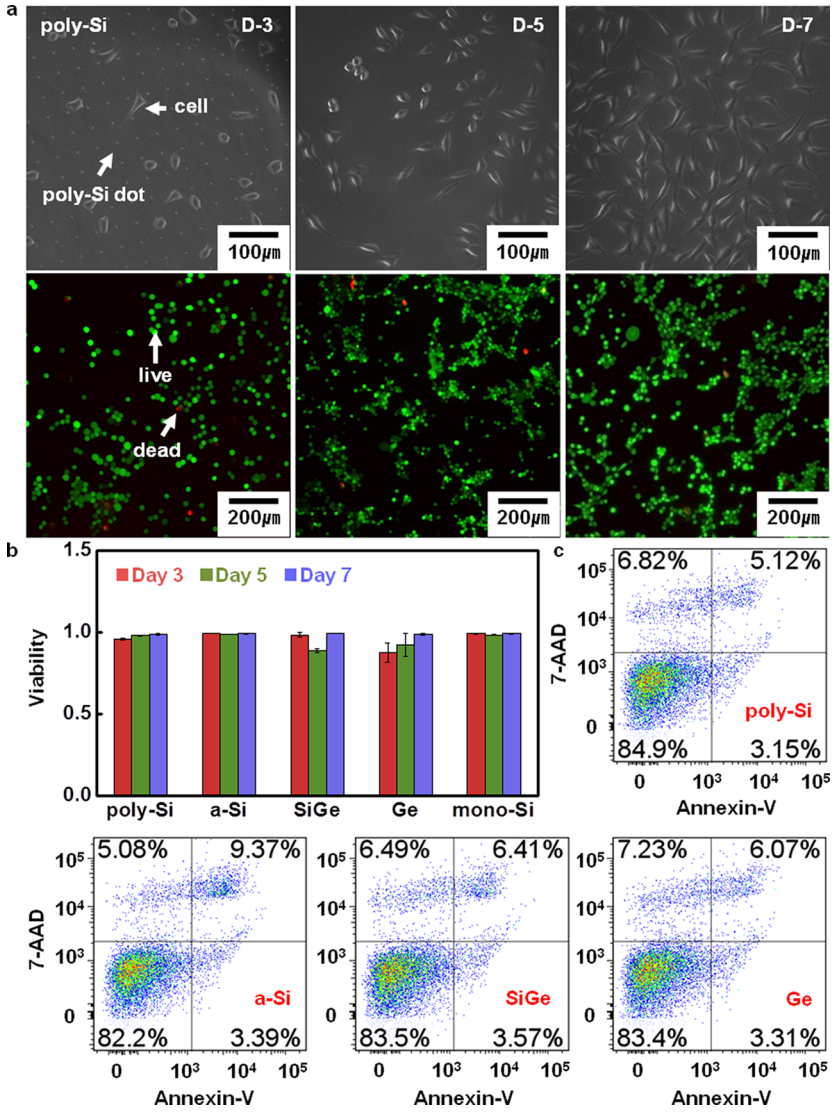

Figure 3. In vitro cell culture evaluations of cytotoxicity of various semiconductors. (a) Differential interference contrast images (top) and fluorescent images (bottom) showing the dissolution behavior and cell viability of poly-Si. Green/red in the fluorescent image represent live/dead cells (L929), respectively. (b) Cell viability of poly-Si, a-Si, SiGe, and Ge over 3, 5, and 7 days calculated as the fraction of total living cells. (c) Estimation of apoptotic populations in L929 after 72 h of culture on poly-Si, a-Si, SiGe, and Ge by Annexin V and 7-AAD, stained using flow cytometry.

immerse samples of poly-Si, a-Si, SiGe, Ge, and mono-Si (designs like those in the dissolution tests) for 24 h at 37 °C. Investigations involved L929 cells incubated for 24 h with various concentrations (up to 100%) of these extracts. The 3-(4,5-dimethylthiazol-2-yl)-2,5-diphenyl-2*H*-tetrazolium bromide (MTT) assay, which measures the reduction of yellow MTT tetrazolium salt to purple formazan as a marker of metabolic activity, defined the viability of the L929 cells.[38] Figure S8a in the SI shows phase-contrast microscope images of cells treated with 100% extract for 72 h. No significant morphological signs of damage appear for extracts from poly-Si, a-Si, SiGe, Ge, or mono-Si, similar to negative control samples (HDPE). The results with PU-ZDEC show damaged cell morphology associated with toxicity, as expected for this positive control. Figure S8b in the SI indicates >95% relative viability of all cells exposed to 75% and 100% extracted supernatants, respectively, suggesting the nontoxic nature of poly-Si, a-Si, mono-Si, SiGe, and Ge compared to HDPE controls. (The relative viability is calculated by setting the viability of the no-device control as 1.)

2.3. Transient Thin-Film Solar Cell. Results from the dissolution studies suggest that these semiconductor materials are excellent candidates for transient biocompatible devices of various types. Fully transient thin-film a-Si solar cells serve as examples (see Figure 4a,b). A 230 nm layer of hydrogenated a-Si (Si:H) with a PIN doping profile (n-region, 20 nm thick, $\sim 10^{20}$ cm^{-3} phosphorus-doped; i-region, 200 nm thick, undoped; p-region, 10 nm thick, $\sim 10^{20}$ cm^{-3} boron-doped), formed by plasma-enhanced chemical vapor deposition (PECVD), severs as the active material. A sputter-deposited film of ZnO with Al dopant (ZnO/Al, ~100 nm thick) provides a transparent conductive oxide (TCO). Mg (~300 nm thick), a representative biodegradable metal, serves as the top and bottom electrodes.

Figure 4c shows a comparison of the current densities of a-Si:H solar cells formed with different combinations of transient and nontransient materials. The reference nontransient cell

DOI: 10.1021/acsami.5b02526
ACS Appl. Mater. Interfaces 2015, 7, 9297−9305

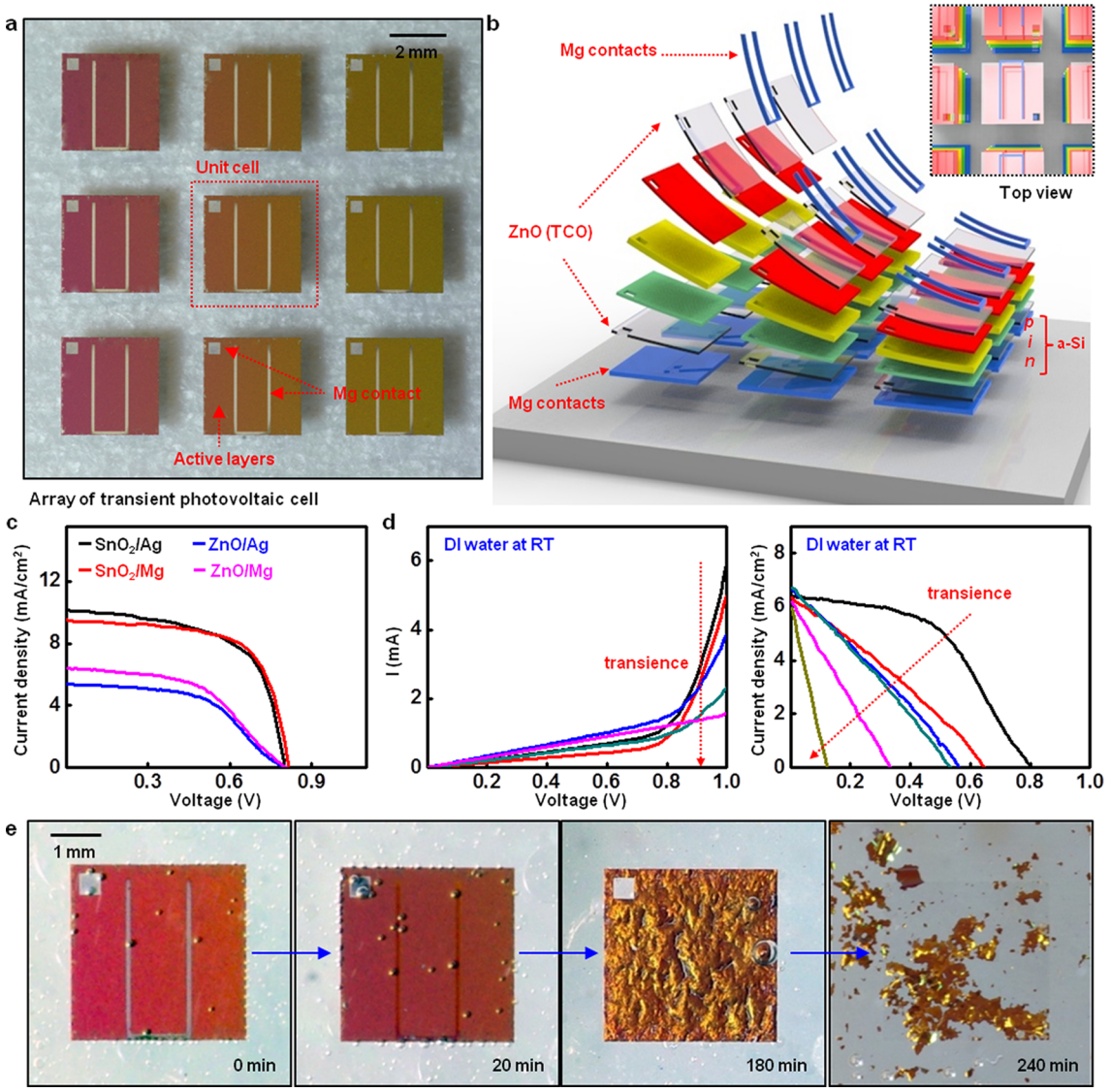

Figure 4. Structure and electrical performance of transient thin-film solar cells that use amorphous silicon (a-Si) active layers. (a) Image of an array of thin-film solar cells (total thickness ~1 μm). (b) Schematic exploded view and top view (inset) illustration of dissolvable transient solar cells. The unit cell consists of Mg electrodes (~300 nm thick), ZnO TCO (~100 nm thick), and an a-Si:H photovoltaic cell (n-region, 20 nm thick; i-region, 200 nm thick; p-region, 10 nm thick). (c) Comparison of the electrical characteristics of a transient a-Si:H solar cell with a nontransient a-Si:H solar cell (Ag metal electrodes and SnO_2:F TCO; black, SnO_2/Ag; red, SnO_2/Mg; blue, ZnO/Ag; purple, ZnO/Mg). (d) Functional transience of a PIN diode (left) and a photovoltaic cell (right) in deionized water at room temperature. The current and efficiency of the cell rapidly decrease as the conductive layer quickly dissolves. Measurements were performed every 10 min after immersion. (e) Optical images at various stages of dissolution of a thin a-Si:H solar cell. The conducting layers of Mg and ZnO dissolve over several hours, followed by complete dissolution of a-Si films within days.

uses fluorine-doped tin oxide (SnO_2:F) and Ag for the TCO and electrodes, respectively. The efficiency (η), open-circuit voltage (V_{oc}), and short-circuit current density (J_{sc}) are 4.9%, 0.80 V, and 10.1 mA/cm^2, respectively. Replacing Ag with Mg yields devices with similar performance (η = 4.8%, V_{oc} = 0.81 V, and J_{sc} = 9.5 mA/cm^2). Cells that use a ZnO/Al for the TCO exhibit η = 2.3%, V_{oc} = 0.80 V, and J_{sc} = 5.45 mA/cm^2 with Ag electrodes and η = 2.6%, V_{oc} = 0.81 V, and J_{sc} = 6.4 mA/cm^2 with Mg electrodes. The cell with SnO_2:F has enhanced performance primarily because of improved conductivity and management of backscattered light (i.e., SnO_2:F presents a patterned surface to increase light absorption; ASAHI Glass, Japan).

Figure 4d summarizes measurements of the performance during hydrolysis of a fully transient a-Si:H solar cell, with contact to the top metal established with a probe tip directly through the solution and contact to the bottom metal through an extended metal trace not directly immersed. The behaviors degrade rapidly primarily because of dissolution of the electrode metal (Mg), on time scales comparable to those of previously reported transient diodes.[1,5] The photovoltaic functionality decreases in a corresponding manner. As the materials dissolve, the short-circuit current density persists even after the disappearance of Mg because of conduction through the ZnO/Al layer. The open-circuit voltage rapidly decreases. Figure 4e shows images at various stages of dissolution. Because of the relatively slow dissolution of a-Si:H compared to ZnO or Mg, disintegration occurs as ZnO and/or Mg disappears because of diffusion of the solution into the multilayer stack. The a-Si:H layer dissolves at a slightly different rate compared

DOI: 10.1021/acsami.5b02526
ACS Appl. Mater. Interfaces 2015, 7, 9297−9305

to the results of thin films of a-Si, likely because of differences in the deposition methods.[6]

3. CONCLUSION

The results presented here provide some understanding of dissolution by hydrolysis of p-Si, a-Si, SiGe, and Ge for applications in bioresorbable forms of transient electronics, including the dependence of the dissolution rates on the temperature and pH. In vitro cytotoxicity evidence suggests that these materials and the products of their dissolution are biocompatible, thereby indicating their potential for use in temporary biomedical devices. A demonstration device consisting of a fully dissolvable thin-film solar cell illustrates the ability to integrate these materials into functional systems by combining them with appropriately selected metals, dielectrics, and other necessary layers.

4. EXPERIMENTAL SECTION

4.1. Dissolution Experiments. Low-pressure chemical vapor deposition formed layers of polycrystalline silicon (poly-Si; ∼100 μm) and amorphous silicon (a-Si; ∼100 μm) on thermal oxide on a Si(100) wafer. Square pads (3 μm × 3 μm) of poly-Si and a-Si were fabricated by photolithography and reactive ion etching (RIE). Monocrystalline silicon−germanium [Si_8Ge_2(100)] and germanium [Ge(100)] wafers were purchased from MTI Corp. (USA). Electron-beam (E-beam) evaporation formed a Ti mask layer (∼30 nm thick) on SiGe and Ge. Patterning a layer of photoresist (S1805, MicroChem, USA) on the Ti, etching the exposed regions with buffered oxide etchant (BOE, 6:1, Transene Co. Inc., USA), and then removing the photoresist yielded a pattern of Ti with an array of square openings (3 μm × 3 μm). For testing, the samples were placed into various types of aqueous solutions (50 mL) including buffer solutions (Sigma-Aldrich, USA) of different pH concentrations (pH 7−10) and bovine serum (Sigma-Aldrich, USA) at room temperature or physiological temperature (37 °C). In all cases, removing the samples from the solutions, rinsing them with deionized water, and then measuring them by atomic force microscopy (AFM; Asylum Research MFP-3D, USA) yielded the thicknesses and surface morphologies at different stages of dissolution.

4.2. Cell Culture and Live/Dead Assay. Mouse fibroblasts from a clone of strain L (NCTC clone 929, KCLB-10001; KCLB, Korea) were cultured in a supplemented Eagle's minimum essential medium (MEM; 10% fetal bovine serum, 4 mM L-glutamate, 100 units/mL penicillin, and 100 g/mL streptomycin) and incubated at 37 ± 2 °C in a humidified atmosphere with 5% CO_2. Primary cultures of splenocytes were obtained from C57BL/6 mice. Splenocytes were cultured in RPMI-1640 (Welgene, Deagu, Korea) supplemented with 5% fetal bovine serum, antibiotics (penicillin 100 U/ml, streptomycin 100 μg/mL), 1X NEAA (Lonza Walkersville Inc., USA), 10 mM HEPES buffer, 1 mM sodium pyruvate (Cellgro, USA), 55 M 2-ME (Gibco, USA), 100 U/mL interleukin-2 (NIH, USA). Cells were placed on the samples at a seeding density of 300 cells/mm^2. The cell viability for the reference materials was assessed qualitatively via the live/dead assay kit (Invitrogen, U.K.). A total of 2 mL of phosphate-buffered saline containing 2.5 μL/mL of 4 μM ethidium homodimer-1 (EthD-1) assay solution and 1 μL/mL of 2 μM calcein AM assay solution was prepared. Calcein appears green in the presence of esterase activity in viable cells, whereas EthD-1 appears red at damaged cell membranes. After the cells were incubated for 30 min at room temperature, they were imaged immediately via fluorescence microscopy (Zeiss Axiovert 200M, Carl Zeiss). The numbers of viable and dead cells in at least three randomly chosen fields were counted and averaged to yield the final result.

4.3. Flow Cytometry with Annexin V/7-AAD. Annexin V and 7-aminoactinomycin D(7-AAD) (Annexin V-FITC Apoptosis detection kit I, BD Biosciences, USA) were used to detect cell death by flow cytometry [FACSCantoII analyzer (BD Biosciences, USA)].[39,40] The data were interpreted with *FlowJo* software (Three Star, USA). The use of annexin V and 7-AAD allowed further discrimination between early apoptotic cells (annexin V+, 7-AAD−), late apoptotic cells (annexin V+, 7-AAD+), and necrotic cells (annexin V−, 7-AAD+), as well as viable cells (annexin V negative, 7-AAD negative).

4.4. Cytotoxicity Assays. Extracts were prepared, at a ratio of 6 cm^2 of sample surface area to 1 mL of culture medium, by extracting samples for 24 h at 37 °C. L-929 mouse fibroblasts (10000 cells/well) were precultured for 24 h in 96-well plates and treated with various concentrations (100%, 75%, 50%, 25%, and 12.5%) of the reference material extracts for 24 h. The cells were incubated for 4 h with 1 mg/mL MTT solutions [3-(4,5-dimethylthiazol-2-yl)-2,5-diphenyl-2*H*-tetrazolium bromide; Sigma, USA] under cell culture conditions. The MTT solution was decanted, and 100 μL of dimethyl sulfoxide was added to each well to dissolve the internalized purple formazan crystals. Absorbances at 570 and 650 nm wavelengths were measured using a microplate spectrophotometer (iMark, Bio-RAD). The results are expressed as a percentage of the absorbance of the control. The viability of splenocytes in the presence of reference materials was measured by Cell Counting Kit-8 (CCK-8; Dojindo Laboratories, Kumamoto, Japan) according to the manufacturer's instructions. Briefly, splenocytes were incubated with samples on 24-well plates for 72 h before the addition of 10% CCK-8 solution. The absorbance at 450 nm was measured by a microplate spectrophotometer (iMark, Bio-Rad). The results correspond to the mean ± standard error of the mean.

4.5. Fabrication/Characterization of Transient a-Si:H Solar Cells. A sequence of deposition and etching of Al-doped ZnO, hydrogenated a-Si, and Mg built transient a-Si:H solar cells. E-beam evaporation and sputtering formed the bottom Mg electrodes (∼300 nm) and Al-doped ZnO (ZnO:Al, ∼100 nm), respectively. Deposition of hydrogenated amorphous silicon (a-Si:H, n-type; ∼20 nm, i-type; ∼200 nm, p-type; ∼10 nm) through 13.56 MHz PECVD yielded the PIN junction. ZnO/Al was deposited on a-Si by sputtering. Patterning the boundary of the unit cell (3.4 mm × 3.4 mm) by photoresist (AZ 4620, MicroChem, USA) and etching the top/bottom ZnO, a-Si:H, and bottom Mg layers by HCl (H_2O/HCl = 50/1), RIE, and $C_2H_4O_2$ (100:1) defined the unit cells. The same patterning and etching process on top/bottom ZnO and a-Si:H layer formed the bottom metal contact. E-beam evaporation of Mg electrodes (∼300 nm) on ZnO yielded the top metal contact. Measurements of *I*−*V* characteristics were performed with a solar simulator (AM 1.5, Newport Corp., USA) and Keithley 2400 (Keithley Instruments, USA).

■ ASSOCIATED CONTENT

Ⓢ Supporting Information

Hydrolysis mechanism of Si, Ge, Mg, Zn, Mo, W, SiO_2, Si_3N_4, and MgO and supplementary figures. This material is available free of charge via the Internet at http://pubs.acs.org.

■ AUTHOR INFORMATION

Corresponding Authors

*E-mail: jcleegm@illinois.edu (J.C.L.).
*E-mail: kyunglee@korea.ac.kr (K.-M.L.).
*E-mail: jrogers@illinois.edu (J.A.R.).

Present Address

◇Department of Civil and Environmental Engineering, Department of Mechanical Engineering, Center for Engineering and Health, and Skin Disease Research Center, Northwestern University, Evanston, Illinois 60208, USA

Author Contributions

‡The manuscript was written through contributions of all authors. All authors have given approval to the final version of the manuscript. These authors (S.-K.K., G.P., and K.K.) contributed equally.

DOI: 10.1021/acsami.5b02526
ACS Appl. Mater. Interfaces 2015, 7, 9297−9305

Funding

The research was funded by an NSF INSPIRE grant awarded to J.A.R. This work was supported by the Basic Science Research Program through the National Research Foundation of Korea (NRF) funded by the Ministry of Science, ICT, and Future Planning (Grants NRF-2007-00107 and NRF-2013M3A9D3045719) awarded to K.-M.L.

Notes

The authors declare no competing financial interest.

■ ACKNOWLEDGMENTS

H.C. is a Howard Hughes Medical Institute International Student Research fellow.

■ REFERENCES

(1) Hwang, S.-W.; Tao, H.; Kim, D.-H.; Cheng, H.; Song, J.-K.; Rill, E.; Brenckle, M. A.; Panilaitis, B.; Won, S. M.; Kim, Y.-S.; Song, Y. M.; Yu, K. J.; Ameen, A.; Li, R.; Su, Y.; Yang, M.; Kaplan, D. L.; Zakin, M. R.; Slepian, M. J.; Huang, Y.; Omenetto, F. G.; Rogers, J. A. A Physically Transient Form of Silicon Electronics. *Science* **2012**, *337*, 1640−1644.

(2) Hwang, S.-W.; Park, G.; Cheng, H.; Song, J.-K.; Kang, S.-K.; Yin, L.; Kim, J.-H.; Omenetto, F. G.; Huang, Y.; Lee, K.-M.; Rogers, J. A. Materials for High-Performance Biodegradable Semiconductor Devices. *Adv. Mater.* **2014**, *26*, 1992−2000.

(3) Dagdeviren, C.; Hwang, S.-W.; Su, Y.; Kim, S.; Cheng, H.; Gur, O.; Haney, R.; Omenetto, F. G.; Huang, Y.; Rogers, J. A. Transient, Biocompatible Electronics and Energy Harvesters Based on ZnO. *Small* **2013**, *9*, 3398−3404.

(4) Yin, L.; Cheng, H.; Mao, S.; Haasch, R.; Liu, Y.; Xie, X.; Hwang, S.-W.; Jain, H.; Kang, S.-K.; Su, Y.; Li, R.; Huang, Y.; Rogers, J. A. Dissolvable Metals for Transient Electronics. *Adv. Funct. Mater.* **2014**, *24*, 645−658.

(5) Kang, S.-K.; Hwang, S.-W.; Yu, S.; Seo, J.-H.; Corbin, E. A.; Shin, J.; Wie, D. S.; Bashir, R.; Ma, Z.; Roges, J. A. Biodegradable Thin Metal Foils and Spin-On Glass Materials for Transient Electronics. *Adv. Funct. Mater.* DOI: 10.1002/adfm.201403469.

(6) Kang, S.-K.; Hwang, S.-W.; Cheng, H.; Yu, S.; Kim, B. H.; Kim, J.-H.; Huang, Y.; Rogers, J. A. Dissolution Behaviors and Applications of Silicon Oxides and Nitrides in Transient Electronics. *Adv. Funct. Mater.* **2014**, *24*, 4427−4434.

(7) Hwang, S.-W.; Park, G.; Edwards, C.; Corbin, E. A.; Kang, S.-K.; Cheng, H.; Song, J.-K.; Kim, J.-H.; Yu, S.; Ng, J.; Lee, J. E.; Kim, J.; Yee, C.; Bhaduri, B.; Su, Y.; Omennetto, F. G.; Huang, Y.; Bashir, R.; Goddard, L.; Popescu, G.; Lee, K.-M.; Rogers, J. A. Dissolution Chemistry and Biocompatibility of Single-Crystalline Silicon Nanomembranes and Associated Materials for Transient Electronics. *ACS Nano* **2014**, *8*, 5843−5851.

(8) Hwang, S.-W.; Song, J.-K.; Huang, X.; Cheng, H.; Kang, S.-K.; Kim, B. H.; Kim, J.-H.; Yu, S.; Huang, Y.; Rogers, J. A. High-Performance Biodegradable/Transient Electronics on Biodegradable Polymers. *Adv. Mater.* **2014**, *26*, 3905−3911.

(9) Hwang, S.-W.; Kim, D.-H.; Tao, H.; Kim, T.-I.; Kim, S.; Yu, K. J.; Panilaitis, B.; Jeong, J.-W.; Song, J.-K.; Omenetto, F. G.; Rogers, J. A. Materials and Fabrication Processes for Transient and Bioresorbable High-Performance Electronics. *Adv. Funct. Mater.* **2013**, *23*, 4087−4093.

(10) Hwang, S.-W.; Huang, X.; Seo, J.-H.; Song, J.-K.; Kim, S.; Hage-Ali, S.; Chung, H.-J.; Tao, H.; Omenetto, F. G.; Ma, Z.; Rogers, J. A. Materials for Bioresorbable Radio Frequency Electronics. *Adv. Mater.* **2013**, *25*, 3526−3531.

(11) Acar, H.; Çınar, S.; Thunga, M.; Kessler, M. R.; Hashemi, N.; Montazami, R. Study of Physically Transient Insulating Materials as a Potential Platform for Transient Electronics and Bioelectronics. *Adv. Funct. Mater.* **2014**, *24*, 4135−4143.

(12) Irimia-Vladu, M.; Troshin, P. A.; Reisinger, M.; Shmygleva, L.; Kanbur, Y.; Schwabegger, G.; Bodea, M.; Schwödiauer, R.; Mumyatov, A.; Fergus, J. W.; Razumov, V. F.; Sitter, H.; Sariciftci, N. S.; Bauer, S. Biocompatible and Biodegradable Materials for Organic Field-Effect Transistors. *Adv. Funct. Mater.* **2010**, *20*, 4069−4076.

(13) Irimia-Vladu, M.; Głowacki, E. D.; Voss, G.; Bauer, S.; Sariciftci, N. S. Green and Biodegradable Electronics. *Mater. Today* **2012**, *15*, 340−346.

(14) Irimia-Vladu, M. "Green" Electronics: Biodegradable and Biocompatible Materials and Devices for Sustainable Future. *Chem. Soc. Rev.* **2013**, *43*, 588−610.

(15) Meredith, P.; Bettinger, C. J.; Irimia-Vladu, M.; Mostert, A. B.; Schwenn, P. E. Electronic and Optoelectronic Materials and Devices Inspired by Nature. *Rep. Prog. Phys.* **2013**, *76*, 034501.

(16) Bettinger, C. J.; Bao, Z. Organic Thin-Film Transistors Fabricated on Resorbable Biomaterial Substrates. *Adv. Mater.* **2010**, *22*, 651−655.

(17) Bettinger, C. J.; Bao, Z. Biomaterials-based Organic Electronic Devices. *Polym. Int.* **2010**, *59*, 563−567.

(18) Hernandez, H. L.; Kang, S.-K.; Lee, O. P.; Hwang, S.-W.; Kaitz, J. A.; Inci, B.; Park, C. W.; Chung, S.; Sottos, N. R.; Moore, J. S.; Rogers, J. A.; White, S. R. Triggered Transience of Metastable Poly(phthalaldehyde) for Transient Electronics. *Adv. Mater.* **2014**, *26*, 7637−7642.

(19) Tao, H.; Hwang, S.-W.; Marelli, B.; An, B.; Moreau, J. E.; Yang, M.; Brenckle, M. A.; Kim, S.; Kaplan, D. L.; Rogers, J. A.; Omenetto, F. G. Silk-based Resorbable Electronic Devices for Remotely Controlled Therapy and In Vivo Infection Abatement. *Proc. Natl. Acad. Sci. U.S.A.* **2014**, *111*, 17385−17389.

(20) Park, J.-H.; Gu, L.; Maltzahn, G. V.; Ruoslahti, E.; Bhatia, S. N.; Sailor, M. J. Biodegradable Luminescent Porous Silicon Nanoparticles for In Vivo Applications. *Nat. Mater.* **2009**, *8*, 331−336.

(21) Laughner, J. I.; Marrus, S. B.; Zellmer, E. R.; Weinheimer, C. J.; MacEwan, M. R.; Cui, S. X.; Nerbonne, J. M.; Efimov, I. R. A Fully Implantable Pacemaker for the Mouse: From Battery to Wireless Power. *PLoS One* **2013**, *23*, 76291.

(22) Chen, L. Y.; Tee, B. C.-K.; Chortos, A. L.; Schwartz, G.; Tse, V.; Lipomi, D. J.; Wong, H.-S. P.; McConnell, M. V.; Bao, Z. Continuous Wireless Pressure Monitoring and Mapping with Ultra-Small Passive Sensors for Health Monitoring and Critical Care. *Nat. Commun.* **2014**, *5*, 5028.

(23) Kamins, T. *Polycrystalline Silicon for Integrated Circuits and Displays*; Kluwer Academic Publishers: Norwell, MA, 1998.

(24) Carlson, D. E.; Wronski, C. R. Amorphous Silicon Solar Cells. *Appl. Phys. Lett.* **1976**, *28*, 671−673.

(25) Vrijen, R.; Yablonovitch, E.; Wang, K.; Jiang, H. W.; Balandin, A.; Roychowdhury, V.; Mor, T.; Divincenzo, D. Electron-Spin-Resonance Transistors for Quantum Computing In Silicon-Germanium Heterostructures. *Phys. Rev. A* **2000**, *62*, 012306.

(26) Szweda, R. *Silicon Germanium Materials & Devices*; Elsevier: New York, 2002.

(27) Wang, Q.; Javey, A.; Tu, R.; Dai, H.; Hyoungsub, K.; McIntyre, P. C.; Krishnamohan, T.; Saraswat, K. C. Germanium Nanowire Field-Effect Transistors with SiO_2 and High-κ HfO_2 Gate Dielectrics. *Appl. Phys. Lett.* **2003**, *83*, 2432.

(28) Harvey, W. W.; Gatos, H. C. The Reaction of Germanium with Aqueous Solutions: I. Dissolution Kinetics in Water Containing Dissolved Oxygen. *J. Electrochem. Soc.* **1958**, *105*, 654−660.

(29) Yin, L.; Farimani, A. B.; Min, K.; Vishal, N.; Lam, J.; Lee, Y. K.; Aluru, N. R.; Rogers, J. A. Mechanisms for Hydrolysis of Silicon Nanomembranes as Used in Bioresorbable Electronics. *Adv. Mater.* **2015**, *27*, 1857−1864.

(30) Seidel, H.; Csepregi, L.; Heuberger, A.; Baumgartel, H. Anisotropic Etching of Crystalline Silicon in Alkaline Solutions. *J. Electrochem. Soc.* **1990**, *137*, 3612−3626.

(31) Borenstein, J. T.; Gerrish, N. D.; Currie, M. T.; Fitzgerald, E. A. A New Ultra Layer for High Precision Micromachining. *IEEE Micro Electro Mech. Syst.* **1999**, 205−210.

(32) Ghodssi, R.; Lin, P. *MEMS Materials and Processes Handbook*; Springer: New York, 2011.

DOI: 10.1021/acsami.5b02526
ACS Appl. Mater. Interfaces 2015, 7, 9297−9305

(33) Bhattacharjeea, S.; Rietjens, I. M. C. M.; Singh, M. P.; Atkins, T. M.; Purkait, T. K.; Xu, Z.; Regli, S.; Shukaliak, A.; Clark, R. J.; Mitchell, B. S.; Alink, G. M.; Marcelis, A. T. M.; Fink, M. J.; Veinot, J. G. C.; Kauzlarich, S. M.; Zuilhof, H. Cytotoxicity of Surface-Functionalized Silicon and Germanium Nanoparticles: the Dominant Role of Surface Charges. *Nanoscale* **2013**, *5*, 4870.
(34) Bayliss, S.; Buckberry, L.; Harris, P.; Rousseau, C. Nanostructured Semiconductors: Compatibility with Biomaterials. *Thin Solid Films* **1997**, *297*, 308−310.
(35) Schmid, I.; Uittenbogaart, C.; Jamieson, B. D. Live-cell Assay for Detection of Apoptosis by Dual-Laser Flow Cytometry using Hoechst 33342 and 7-Amino-Actinomycin. *Nat. Protoc.* **2007**, *1*, 187−190.
(36) *Biological Evaluation for Medical Device, part 5. Test for Cytotoxicity: In Vitro Methods*, 1992; ISO 10993.
(37) Scarisbrick, I. A.; Epstein, B.; Cloud, B. A.; Yoon, H.; Wu, J.; Renner, D. N.; Blaber, S. I.; Blaber, M.; Vandell, A. G.; Bryson, A. L. Functional Role of Kallikrein 6 in Regulating Immune Cell Survival. *PLoS One* **2011**, *6*, e18376.
(38) Park, G.; Chung, H. J.; Kim, K.; Lim, S. A.; Kim, J.; Kim, Y. S.; Liu, Y.; Yeo, W. H.; Kim, R. H.; Kim, S. S.; Kim, J.-S.; Jung, Y. H.; Kim, T.-I.; Yee, C.; Rogers, J. A.; Lee, K.-M. Immunologic and Tissue Biocompatibility of Flexible/Stretchable Electronics and Optoelectronics. *Adv. Healthcare Mater.* **2014**, *3*, 515−525.
(39) Erika, A. O. D.; David, N. E.; Ravi, H. Multiparameter Flow Cytometry: Advances in High Resolution Analysis. *Immune Netw.* **2013**, *13*, 43−54.
(40) Song, I. S.; Jeong, Y. J.; Jeong, S. H.; Heo, H. J.; Kim, H. K.; Lee, S. R.; Ko, T. H.; Youm, J. B.; Kim, N.; Ko, K. S.; Rhee, B. D.; Han, J. Combination Treatment with 2-Methoxyestradiol Overcomes Bortezomib Resistance of Multiple Myeloma Cells. *Exp. Mol. Med.* **2013**, *45*, e50.

DOI: 10.1021/acsami.5b02526
ACS Appl. Mater. Interfaces 2015, 7, 9297−9305